

# Polyoxometalate-Based Metal–Organic Frameworks for Selective Oxidation of Aryl Alkenes to Aldehydes

Yuanyuan Ma,<sup>†</sup> Haiyue Peng,<sup>†</sup> Jianing Liu,<sup>†</sup> Yonghui Wang,<sup>\*,†</sup> Xiuli Hao,<sup>†,‡</sup> Xiaojia Feng,<sup>†,§</sup> Shifa Ullah Khan,<sup>†</sup> Huaqiao Tan,<sup>\*,†</sup> and Yangguang Li<sup>\*,†</sup>

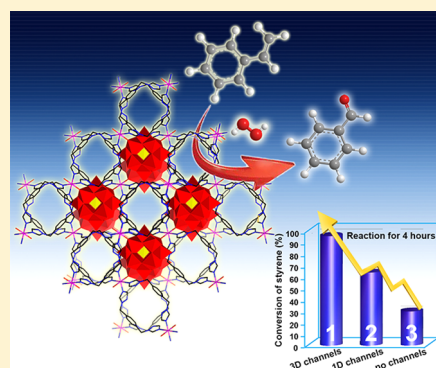
<sup>†</sup>Key Laboratory of Polyoxometalate Science of Ministry of Education Faculty of Chemistry, Northeast Normal University, Changchun 130024, China

<sup>‡</sup>School of Chemical and Biological Engineering, Taiyuan University of Science and Technology, Taiyuan 030021, China

<sup>§</sup>College of Science, Shenyang Agricultural University, Shenyang 110866, China

## Supporting Information

**ABSTRACT:** Polyoxometalates (POMs) show considerable catalytic performance toward the selective oxidation of alkenes to aldehydes, which is commercially valuable for the production of pharmaceuticals, dyes, perfumes, and fine chemicals. However, the low specific surface area of POMs as heterogeneous catalysts and poor recyclability as homogeneous catalysts have hindered their wide application. Dispersing POMs into metal–organic frameworks (MOFs) for the construction of POM-based MOFs (POMOFs) suggests a promising strategy to realize the homogeneity of heterogeneous catalysis. Herein, we report two new POMOFs with chemical formulas of  $[\text{Co}(\text{BBTZ})_2][\text{H}_3\text{BW}_{12}\text{O}_{40}] \cdot 10\text{H}_2\text{O}$  (**1**) and  $[\text{Co}_3(\text{H}_2\text{O})_6(\text{BBTZ})_4][\text{BW}_{12}\text{O}_{40}] \cdot \text{NO}_3 \cdot 4\text{H}_2\text{O}$  (**2**) (BBTZ = 1,4-bis(1,2,4-triazol-1-ylmethyl)benzene) for the selective oxidation of alkenes to aldehydes. Compound **1** possesses a non-interpenetrated three-dimensional (3D) *cds*-type open framework with a 3D channel system. Compound **2** displays a 3D polyrotaxane framework with one-dimensional channels along the  $[100]$  direction. In the selective oxidation of styrene into benzaldehyde, compound **1** can achieve a 100% conversion in 4 h with 96% selectivity toward benzaldehyde, which is superior to that of compound **2**. A series of control experiments reveal that the co-role of  $[\text{BW}_{12}\text{O}_{40}]^{5-}$  and  $\text{Co}^{2+}$  active center as well as a more open framework feature co-promote the catalytic property of the POMOFs in this case. This work may suggest a new option for the development of POMOF catalysts in the selective oxidation of alkenes.



## 1. INTRODUCTION

Polyoxometalates (POMs) as a well-defined library of nano-sized metal–oxo clusters have been extensively explored in the field of catalysis, owing to their tunable acidity, high thermal stability, unique redox properties, and inherent resistance to oxidation.<sup>1–5</sup> To maximize the benefit of POMs, the design and synthesis of POM-based metal organic frameworks (POMOFs) have been developed as an efficient strategy that can realize a good dispersal of POMs at the molecular level and can expose more accessible active sites.<sup>6,7</sup> Meanwhile, the appropriate porous structures or channels in POMOFs facilitate the accessibility of reactant molecules to active POM species, actualizing the homogeneity of heterogeneous catalysis. To date, plenty of POMOFs have been reported;<sup>8–13</sup> however, only a few of them were successfully explored as heterogeneous catalysts, and the reaction models catalyzed by POMOFs are still limited since the catalysts usually possess specific activity and selectivity for certain reactions.<sup>11–13</sup> Therefore, it is still a great challenge to design and prepare desired POMOFs according to the requirement of specific catalytic reactions and to expand their catalytic reaction scopes.

Selective oxidation of alkenes to aldehydes is one of the most important and commercially valuable chemical reactions, since aldehydes (especially benzaldehydes) have been widely used for the production of pharmaceuticals, dyes, perfumes, and fine chemicals.<sup>14–17</sup> In this reaction system, POMs have exhibited excellent activity and selectivity as homogeneous catalysts.<sup>7,18</sup> However, the poor recyclability of POM catalysts hindered their further application. The construction of POM-based heterogeneous catalysts usually decreases the catalytic activity due to the low specific surface area and the low exposure of POM active sites. Thus, constructing new POMOF catalysts becomes a feasible strategy for solving the above problem. In order to introduce catalytically active POM units into the POMOFs, we conducted a series of preliminary experimental studies (Table S1 in the Supporting Information), demonstrating that polyoxotungstate-based catalysts exhibit potential catalytic activities on the selective oxidation of styrene to benzaldehydes.<sup>7b,19</sup> Among these catalysts,  $\text{K}_5[\text{BW}_{12}\text{O}_{40}]$  exhibits ideal catalytic activity and selectivity compared to

Received: January 31, 2018

those of  $\text{Na}_3[\text{PW}_{12}\text{O}_{40}]$  and  $\text{K}_4[\text{SiW}_{12}\text{O}_{40}]$ . Meanwhile, the high negative charges of  $\text{K}_5[\text{BW}_{12}\text{O}_{40}]$  are also conducive to construct 3D porous frameworks with the metal–organic coordination fragments.<sup>7</sup> Moreover, considering the unique catalytic activity of the Co element in many oxidation transformations,<sup>20,21</sup> we selected cobalt ions,  $[\text{BW}_{12}\text{O}_{40}]^{5-}$ , and the neutral N-donor bridging ligand (1,4-bis(triazol-1-ylmethyl)benzene (BBTZ)) (Figure S1) to construct new POMOF catalysts for the selective oxidation of alkenes. Herein, we report two new POMOFs:  $[\text{Co}(\text{BBTZ})_2][\text{H}_3\text{BW}_{12}\text{O}_{40}] \cdot 10\text{H}_2\text{O}$  (1) and  $[\text{Co}_3(\text{H}_2\text{O})_6(\text{BBTZ})_4][\text{BW}_{12}\text{O}_{40}] \cdot \text{NO}_3 \cdot 4\text{H}_2\text{O}$  (2). Compound 1 exhibits a 3D open framework with a non-interpenetrated *cds*-type topology. The channels in three directions are interconnected with each other to form a 3D channel system. Compound 2 possesses a 3D polyrotaxane framework with only 1D channels. Compound 1 shows excellent catalytic activity in the selective oxidation of styrene to benzaldehyde and realizes a full conversion of styrene in 4 h with a 96% selectivity toward benzaldehyde, which is superior to that of compound 2. Furthermore, compound 1 demonstrates good compatibility and recyclability in the catalytic reaction system. To our knowledge, compound 1 represents the first POMOF catalyst unleashing the advantage in the oxidation reaction of styrene to benzaldehyde.

## 2. RESULTS AND DISCUSSION

**Crystal Structure of Compound 1.** X-ray single-crystal diffraction analysis revealed that compound 1 crystallizes in the monoclinic system with the  $C2/c$  space group. The crystallographically asymmetric unit is constitutive of one  $\text{Co}^{2+}$  (Co1) ion, two BBTZ bridging ligands, one protonated  $\alpha$ -Keggin-type polyoxoanion  $[\text{H}_3\text{BW}_{12}\text{O}_{40}]^{2-}$ , and ten lattice water molecules (Figure S2). Among them, the Co center (Co1) adopts a six-coordinated mode by connecting to four nitrogen atoms originating from four BBTZ ligands and two O atoms derived from two  $[\text{H}_3\text{BW}_{12}\text{O}_{40}]^{2-}$  units (Figure S2). The Co–N bond distance ranges from 2.057(13) to 2.073(14) Å, and the bond lengths of Co–O are 2.303(15) Å. The O/N–Co–N/O bond angles vary from 89.4(6)° to 180° (Table S2). In compound 1, the BBTZ ligands adopt only a *cis*-type configuration, which are coordinated to the adjacent two Co centers into 1D loop-containing chains (Figure 1a). The ligands in the loop units can be considered as linkers. The  $[\text{H}_3\text{BW}_{12}\text{O}_{40}]^{2-}$  units can be also viewed as linkers which are connected by adjacent Co centers to form into POM-containing chains (Figure 1a). These loop-containing 1D chains and POM-containing chains are further perpendicularly connected with each other, forming a rare non-interpenetrated 3D four-connected  $\{6^5.8\}$  net with the  $\text{CdSO}_4$  (*cds*) topology (Figure 1b). The open framework of compound 1 contains a 3D channel system (Figure 1c). These channels intersect with each other and extend in three different directions (Figures 2 and S3–S5). The window size is 8.50(7) Å  $\times$  8.50(7) Å along the [001] direction, 6.31(1) Å  $\times$  5.47(9) Å along the [110] direction, and 6.31(1) Å  $\times$  5.47(9) Å along the  $[\bar{1}\bar{1}0]$  direction, as shown in Figures S3–S5. It is worth noting that the channels with the window size of 8.50(7) Å  $\times$  8.50(7) Å are hydrophobic and the other two kind of channels are hydrophilic, which could be a benefit for the entrance and reaction of organic substrates and  $\text{H}_2\text{O}_2$  molecules (Figure 2). For compound 1, the solvent accessible volume is ca. 28.9% based on the calculation of the PLATON program.<sup>22</sup> Such an open framework realizes the good

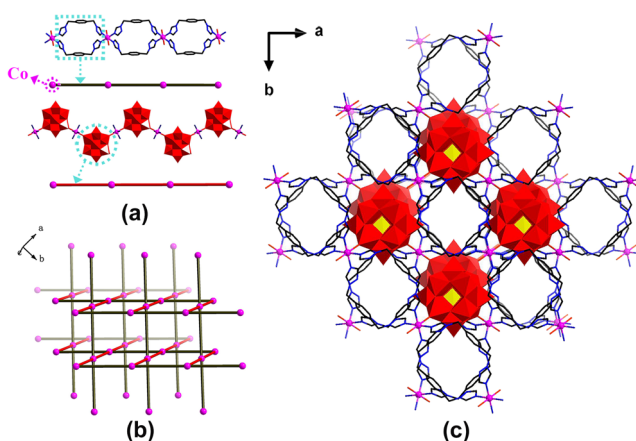


**Figure 1.** (a) Ball-and-stick and schematic views of the basic building units (1D loop-containing chains and POM chains) in the structure of compound 1. (b) Schematic view of the *cds*-type framework in compound 1. (c) Ball-and-stick and polyhedral views of the 3D open framework in compound 1 viewed along the *c* axis.

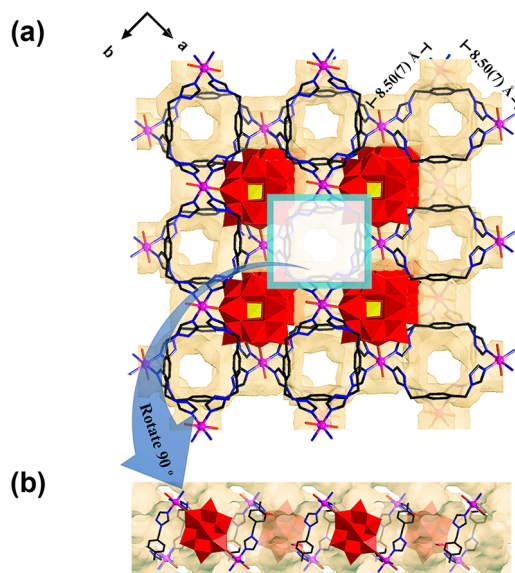


**Figure 2.** (a) Ball-and-stick and polyhedral views of the 3D open framework of compound 1 with 3D channels viewed along the *c* axis. (b) The channel along the [001] direction in compound 1. The solvent accessible voids are modeled with a yellow background.

dispersion of POMs and exposes more active sites for heterogeneous catalysis.

**Crystal Structure of Compound 2.** Compound 2 crystallizes in the triclinic system with a  $P\bar{1}$  space group. The crystallographically asymmetric unit is constitutive of one  $[\text{BW}_{12}\text{O}_{40}]^{5-}$  polyoxoanion, three  $\text{Co}^{2+}$  (one Co1, two Co2) ions, four BBTZ ligands, six coordinated water molecules connected to two Co2 centers, four lattice water molecules, and a  $\text{NO}_3^-$  ion (Figure S6). The valence states of Co and W have been confirmed by bond valence sum (BVS) calculations and X-ray photoelectron spectra (XPS) (Table S3 and Figure S7). In compound 2, two kinds of metal–organic coordination polymer moieties exist in the structure, that is, the 2D network units and the 0D loops (Figure 3). The 2D network holds one Co center (Co1), which displays a hexa-coordinated octahedral configuration surrounded by two O atoms from two  $[\text{BW}_{12}\text{O}_{40}]^{5-}$  units and four N atoms originating from four

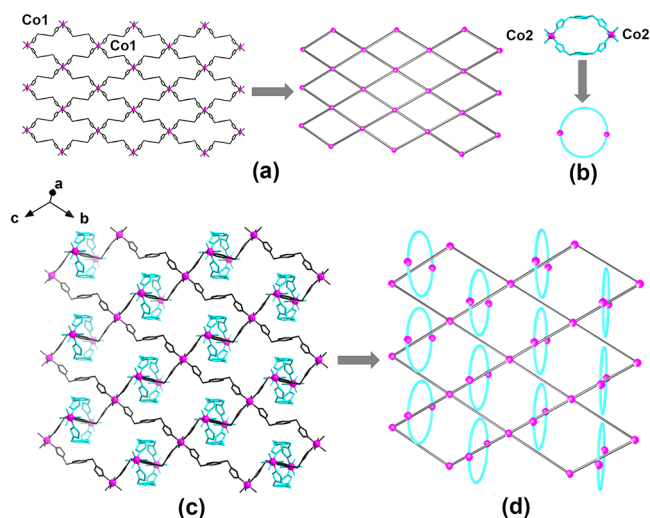


**Figure 3.** (a, b) Ball-and-stick and schematic views of the 2D metal–organic network unit and 0D loop unit in compound **2**. (c, d) Ball-and-stick and schematic views of the 2D polyrotaxane architecture in compound **2**.

BBTZ ligands (Figure S6). The Co1–N bond distance is in the range of 2.107(8)–2.120(8) Å, and the Co1–O bond length is 2.155(10) Å. The N(O)–Co1–N(O) bond angles are in the range of 89.2(4)–180° (Table S4). In such a 2D network, all of the BBTZ ligands are in *trans* configuration, joining the Co1 centers into a 2D network with 4<sup>+</sup> *sqa* topology (Figure 3a). The 0D loops also contain one Co center (Co2) which exhibits an octahedral coordination geometry, defined by two N atoms from two BBTZ ligands, one O atom from the [BW<sub>12</sub>O<sub>40</sub>]<sup>5-</sup> unit, and three coordinated water molecules (Figures 3b and S6). The bond lengths of Co2–N/O are in the range of 2.110(10)–2.122(10) Å. The bond angles of N(O)–Co2–N(O) are in the range of 90.3(5)–175.8(6)° (Table S4). In this fragment, adjacent Co2 ions are jointed by two *cis* BBTZ ligands, forming 0D loops (Figure 3b). It is noteworthy that the 2D network unit penetrates the 0D loops, exhibiting an interesting polyrotaxane architecture (Figure 3c and 3d). In compound **2**, each [BW<sub>12</sub>O<sub>40</sub>]<sup>5-</sup> unit can be viewed as a four-connection node that is linked with two Co1 atoms from the adjacent 2D nets and two Co2 atoms from two 0D loops (Figure S8). Based on such a connection, the 2D polyrotaxane networks are linked together by POM units, generating a 3D open network (Figures 4a and S9). If the 0D loop is viewed as a linker, while the Co1 center and [BW<sub>12</sub>O<sub>40</sub>]<sup>5-</sup> unit are reduced to six-connected and four-connected nodes, respectively, the whole framework of compound **2** adopts a 4,6-T19 topology with the point symbol {4<sup>2</sup>.6<sup>3</sup>.8}{4<sup>6</sup>.6<sup>9</sup>} (Figures 4b and S9). Such an open framework contains 1D channels with a window size of 10.23(9) Å × 6.62(1) Å along the [100] direction (Figures 4c and S10). The solvent-accessible void in compound **2** is 17% calculated by using the PLATON program.<sup>22</sup>

**Selective Oxidation of Styrene.** Selective oxidation of alkenes into aldehydes is an important commercial reaction since aldehydes have emerged as significant chemical materials and been widely used for the production of pharmaceuticals, dyes, perfumes, and fine chemicals.<sup>23–27</sup> Herein, the selective oxidation of styrene was chosen as a model reaction to evaluate the catalytic activities of POM-based MOF materials. To optimize the reaction conditions, styrene oxidation reactions were first carried out in various solvents at 70 °C using

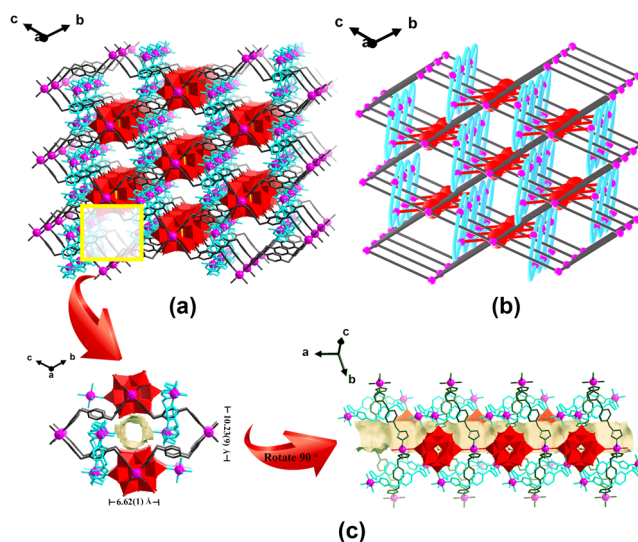


**Figure 4.** (a) Ball-and-stick and polyhedral views of the 3D open framework of compound **2** along the *a* axis. (b) Schematic view of the 3D structural topology in compound **2**. (c) 1D channel in compound **2**. The solvent accessible voids are modeled with a yellow background.

compound **1** as the catalyst and hydrogen peroxide as the oxidant (Tables 1 and S5). As shown in Table 1, the reactions

**Table 1. Optimization of the Different Reaction Conditions for Styrene Oxidation to Benzaldehyde by Using Compound **1** as the Catalyst<sup>a</sup>**

entry	solvent	<i>T</i> (°C)	conv. <sup>b</sup> (%)	select. <sup>b</sup> (%)
1	toluene	70	50 ± 4	77 ± 2
2	ethanol	70	73 ± 2	49 ± 3
3	DMF	70	100	51 ± 1
4	H <sub>2</sub> O	70	91 ± 2	62 ± 3
5	CH <sub>3</sub> CN	70	>99	96 ± 3
6	CH <sub>3</sub> CN	80	>99	73 ± 2
7	CH <sub>3</sub> CN	60	63 ± 3	96 ± 1
8	CH <sub>3</sub> CN	50	34 ± 5	95 ± 1
9	CH <sub>3</sub> CN	40	12 ± 3	94 ± 2

<sup>a</sup>Reaction conditions: styrene (0.25 mmol), H<sub>2</sub>O<sub>2</sub> (1 mmol), catalyst (0.028 mmol), and solvent (2 mL) for 4 h. <sup>b</sup>Determined by GC analysis.

in toluene and ethanol exhibit a low conversion (50% and 73%, respectively) of styrene and low selectivity (77% and 49%, respectively) to benzaldehyde (Table 1, entries 1 and 2, respectively). In DMF and H<sub>2</sub>O, the catalytic reactions achieve a good conversion of styrene, but the selectivity (51% and 62%, respectively) to benzaldehyde is still low (Table 1, entries 3 and 4). In comparison, acetonitrile was the suitable solvent for this reaction to afford a full conversion of styrene and high selectivity of benzaldehyde in 4 h (96%; Table 1, entry 5). The reaction temperature also affects the catalytic performance in this reaction system (Table 1, entries 5–9). With an increase of temperature to 80 °C, the selectivity of benzaldehyde dropped to 70%, which may be due to the over-oxidation of benzaldehyde.<sup>27</sup> Decreasing the temperature to 40 °C led to the decline of the styrene conversion. On the basis of a series of

control experiments, the suitable temperature that can achieve the best conversion and selectivity is 70 °C.

With the aforementioned optimized reaction conditions, we systematically evaluated the catalytic activities of compounds **1** and **2** on the selective oxidation of styrene. When compound **1** was used as the catalyst, the full conversion of styrene was achieved in 4 h with a 96% selectivity to benzaldehyde (Figures S5a and S11; Table 2, entry 1). Using compound **2** as the

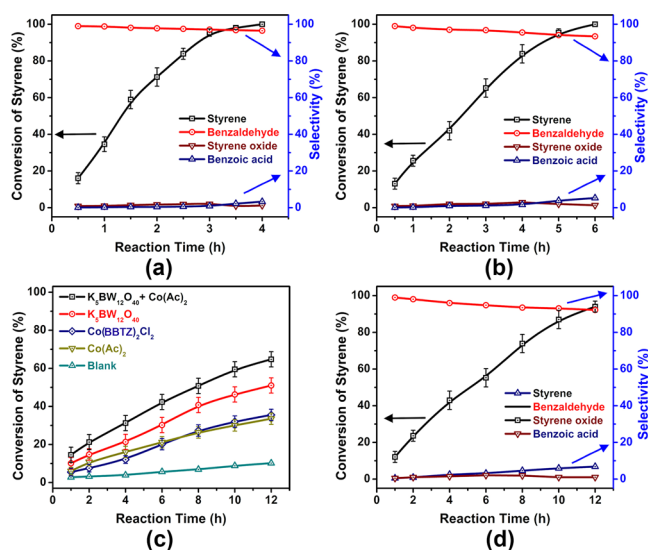


**Figure 5.** Conversion of styrene and selectivity of products in the selective oxidation of styrene with (a) compound **1** and (b) compound **2** as catalysts. (c) The conversion of styrene with a series of control samples as catalysts as a function of reaction time. (d) The conversion of styrene and selectivity of products in the selective oxidation of styrene catalyzed by compound **3**. Reaction conditions: styrene (0.25 mmol), H<sub>2</sub>O<sub>2</sub> (1 mmol), catalysts (0.028 mmol), and acetonitrile (2 mL) at 70 °C.

**Table 2.** Catalytic Oxidation of Styrene to Benzaldehyde with H<sub>2</sub>O<sub>2</sub><sup>a</sup>

entry	catalyst	time (h)	conv. <sup>c</sup> (%)	select. <sup>c</sup> (%)
1	compound <b>1</b>	4	>99	96 ± 3
2	compound <b>2</b>	6	>99	93 ± 2
3	K <sub>5</sub> BW <sub>12</sub> O <sub>40</sub> ·11H <sub>2</sub> O	12	51 ± 2	89 ± 2
4	Co(OAc) <sub>2</sub> ·4H <sub>2</sub> O	12	33 ± 4	91 ± 3
5	K <sub>5</sub> BW <sub>12</sub> O <sub>40</sub> ·11H <sub>2</sub> O Co(OAc) <sub>2</sub> ·4H <sub>2</sub> O <sup>b</sup>	12	64 ± 3	85 ± 2
6	Co(BBTZ) <sub>2</sub> Cl <sub>2</sub>	12	35 ± 3	90 ± 2
7	compound <b>3</b>	12	94 ± 2	92 ± 2

<sup>a</sup>Reaction conditions: styrene (0.25 mmol), H<sub>2</sub>O<sub>2</sub> (1 mmol), catalyst (0.028 mmol), and acetonitrile (2 mL) at 70 °C. <sup>b</sup>Both POM and cobalt salt catalysts are 0.028 mmol. <sup>c</sup>The values are based on GC analysis.

catalyst, the reaction required 6 h to afford the 100% conversion of styrene with a 93% selectivity to benzaldehyde (Figure S5b; Table 2, entry 2). Since both compounds possess a similar composition, the distinction of their catalytic activities should mainly stem from their structural differences. Compound **1** possesses 3D channels, which can expose more active sites than compound **2**.

To illuminate the catalytic active sites in compounds **1** and **2**, a series of contrast experiments were conducted under the same

reaction conditions (Figure S5c and Table 2). Using the same equivalents of POM precursor (K<sub>5</sub>BW<sub>12</sub>O<sub>40</sub>·11H<sub>2</sub>O) as the catalyst, the conversion of styrene was just 51% after 12 h, which is lower than that of both compounds **1** and **2**. The relatively low activity of the POM precursor can be ascribed to its low specific surface area, which hinders the accessibility of the reaction substrate to the active site. The use of a transition-metal precursor (Co(OAc)<sub>2</sub>·4H<sub>2</sub>O) to catalyze this reaction led to a 33% conversion and a 91% selectivity, suggesting that the Co<sup>2+</sup> ion also possesses a relatively high selectivity to benzaldehyde (Figure S5c; Table 2, entries 3–5). Furthermore, Co(BBTZ)<sub>2</sub>Cl<sub>2</sub><sup>28</sup> exhibits a catalytic activity and selectivity similar to those of Co(OAc)<sub>2</sub>·4H<sub>2</sub>O, indicating that the BBTZ ligand makes no contribution in enhancing the catalytic activity of the catalysts (Figures S5c and S12; Table 2, entry 6). A blank experiment in the absence of any catalyst revealed a negligible conversion (<10%) of styrene (Figure S5c). These results demonstrate that both POM units and Co<sup>2+</sup> ions make an important contribution to the high activity and selectivity of compounds **1** and **2**. In order to gain further insight into the structural influence of compounds **1** and **2** on the catalytic performance, we selected another non-porous POM-based organic–inorganic hybrid compound with the chemical formula [Co<sub>2.5</sub>(BBTZ)<sub>4</sub>(H<sub>2</sub>O)] [BW<sub>12</sub>O<sub>40</sub>]·4H<sub>2</sub>O as the reference catalyst **3** for the selective oxidation of styrene.<sup>29</sup> Compound **3** possesses a chemical composition similar to that of compounds **1** and **2** but has no solvent-accessible void in its crystal structure (Figure S13). The catalytic reaction with compound **3** achieved a 100% conversion in 12 h and a 92% selectivity to benzaldehyde, which was obviously slower than the reactions catalyzed by compounds **1** (4 h) and **2** (6 h), but kept a high selectivity (Figure S5d and Table 2, entry 7). This result suggests that styrene oxidation catalyzed by compound **3** just occurs on the surface of the catalyst. As for compounds **1** and **2**, their inherent porous property exposes more catalytic sites both on the external surface and in interior channels, thus accelerating the oxidation reaction.

Furthermore, we expanded the substrate scope in order to investigate the general applicability of the catalytic system. As summarized in Table 3, both electron-withdrawing and electron-donating substrates can be converted smoothly and selectively into corresponding aldehydes by the use of compound **1** as catalyst. 4-Fluorostyrene and 4-chlorostyrene exhibit 95% and 98% conversion after 4 and 6 h, respectively (Table 3, entries 2 and 3, respectively). 4-Nitrostyrene can also be fully converted and generate the corresponding aldehyde with a high selectivity (99%) in 6 h (Table 3, entry 4). 4-Methylstyrene achieved 97% conversion and a 99% selectivity in 6 h (Table 3, entry 5). As for 4-methoxystyrene and 4-isopropylstyrene, a good conversion (>95%) can be obtained after 7 h, and the selectivities corresponding to benzaldehyde are 97% and 94%, respectively (Table 3, entries 6 and 7, respectively). 2-Vinylnaphthalene can also achieve a 94% conversion and a 96% selectivity after 7 h. It is presumed that the different reaction times for the oxidation of various styrene derivatives may be related to the molecular size of the substrates (Figure S14). With the increasing of substrate size, achieving the full conversion requires a longer reaction time. This result suggests that the substrates with a large molecular size may not match the channels in compound **1**, thus decreasing the conversion efficiency. Additionally, compound **2** can also high-selectively catalyze the oxidation of styrene derivatives to the corresponding aldehydes with a much longer

Table 3. Selective Catalytic Oxidation of Styrene Derivatives to the Corresponding Aldehydes with H<sub>2</sub>O<sub>2</sub><sup>a</sup>

Entry	Substrate	Product	Time (h)	Conv. <sup>b</sup> [%]	Select. <sup>b</sup> [%]
1			4	>99	96
2			4	95	98
3			6	98	99
4			6	>99	99
5			6	97	99
6			7	96	97
7			7	95	94
8			7	94	96

<sup>a</sup>Reaction conditions: styrene derivatives (0.25 mmol), H<sub>2</sub>O<sub>2</sub> (1 mmol), catalyst **1** (0.028 mmol), and acetonitrile (2 mL) at 70 °C. <sup>b</sup>The values are based on GC analysis.

reaction time (Table S6). These results further confirm that the pore size of the catalysts has an obvious influence on the catalytic activities in such a selective oxidation of styrene series. Overall, compounds **1** and **2** exhibit an excellent catalytic performance for the selective oxidation of styrene to aldehydes (Table S7).

The recyclability of compound **1** as a heterogeneous catalyst has also been investigated. The catalyst can be easily recovered from the reaction system by centrifugation and reused seven times without significant loss of catalytic activity (Figures S15 and S16). These results demonstrate the good stability and recyclability of compound **1**. PXRD patterns and IR spectra after recycling disclose that compound **1** retains its structural integrity (Figures S17 and S18). The insoluble nature of compound **1** was also examined by a hot filtration experiment (Figure S19). After 2 h of reaction, the catalyst was removed from the reaction system and the filtrate was kept under its original conditions. No further reaction was detected, confirming the heterogeneity of this material. Moreover, the UV–vis spectra of the filtrate also showed that no signal of POM was detected, further confirming the stability of compound **1** (Figure S20).

### 3. CONCLUSION

In summary, we reported two new POMOFs which were utilized in catalyzing the selective oxidation of styrene to aldehydes for the first time and which showed excellent catalytic activity and high selectivity. Compound **1** displays a 3D non-interpenetrated *cds*-type framework with a 3D open channel system. Compound **2** exhibits a 3D polyrotaxane framework with 1D channels. Compound **1** can achieve a 100% conversion of styrene in 4 h with a 96% selectivity toward benzaldehyde, which is superior to that of compound **2**. A series of control experiments demonstrate that both

[BW<sub>12</sub>O<sub>40</sub>]<sup>5-</sup> and Co<sup>2+</sup> catalytically active centers, together with a more open framework of POMOFs, facilitate the selective oxidation of styrene to aldehyde. This work suggests a new option for the development of POMOF catalysts. Engineering large porous POMOFs with catalytically active POM units and extended organic bridging ligands may generate more efficient catalysts for the oxidation of alkenes to aldehydes. This work is ongoing in our group.

### 4. EXPERIMENTAL SECTION

**Materials and Methods.** All commercially available reagents for syntheses were used without further purification. 1,4-Bis(triazol-1-ylmethyl)benzene (BBTZ) as a ligand was synthesized according to a reported procedure.<sup>30</sup> K<sub>5</sub>[α-BW<sub>12</sub>O<sub>40</sub>]·11H<sub>2</sub>O was prepared according to literature methods.<sup>31</sup> [Co<sub>2.5</sub>(H<sub>2</sub>O)<sub>2</sub>(BBTZ)<sub>4</sub>][BW<sub>12</sub>O<sub>40</sub>]·4H<sub>2</sub>O (**3**) has been reported by our group earlier and synthesized based on literature methods.<sup>29</sup> Compound Co(bbtz)<sub>2</sub>Cl<sub>2</sub> was synthesized with reference to the literature methods.<sup>28</sup>

**Synthesis of [Co(BBTZ)<sub>2</sub>][H<sub>3</sub>BW<sub>12</sub>O<sub>40</sub>]·10H<sub>2</sub>O (**1**).** BBTZ (0.205 g, 0.85 mmol) was dispersed in CH<sub>3</sub>CN/H<sub>2</sub>O (10 mL, *v/v* = 3:3) at room temperature, and then K<sub>5</sub>[α-BW<sub>12</sub>O<sub>40</sub>]·11H<sub>2</sub>O (1.29 g, 0.4 mmol) and Co(OAc)<sub>2</sub>·4H<sub>2</sub>O (0.127 g, 0.5 mmol) were added to the solution and stirred for 0.5 h. Then, concentrated HNO<sub>3</sub> (30 μL) was added dropwise to adjust the pH value of the hybrid solution to 1.0. The turbid liquid was transferred to a 23 mL Teflon-lined autoclave and heated at 130 °C for 4 days. After the solution was slowly cooled to room temperature, orange block crystals were obtained and filtered (56% yield based on W). The final pH value of the solution was 2.5. Anal. Calcd for C<sub>24</sub>H<sub>47</sub>N<sub>12</sub>O<sub>50</sub>BW<sub>12</sub>Co: C 8.05, H 1.32, N 4.69, B 0.30, W 61.68, Co 1.65. Found: C 8.17, H 1.41, N 4.72, W 61.64, Co 1.68. Selected IR (solid KBr pellet, cm<sup>-1</sup>): 3370(m), 3111(m), 1621(w), 1523(s), 1426(m), 1371(w), 1284(s), 1217(w), 1132(s), 995(m), 954(s), 914(s), 823(s). TG analysis demonstrates that the first weight loss ranging from 50 to 200 °C can be identified as the loss of ten lattice water molecules (Figure S21).

**Synthesis of [Co<sub>3</sub>(H<sub>2</sub>O)<sub>6</sub>(BBTZ)<sub>4</sub>][BW<sub>12</sub>O<sub>40</sub>]·NO<sub>3</sub>·4H<sub>2</sub>O (**2**).** K<sub>5</sub>[α-BW<sub>12</sub>O<sub>40</sub>]·11H<sub>2</sub>O (1.29 g, 0.4 mmol) and BBTZ (0.144 g, 0.6

mmol) were dispersed in CH<sub>3</sub>CN/H<sub>2</sub>O (10 mL, *v/v* = 2:4) at ambient temperature, and then a mixture of K<sub>5</sub>[α-BW<sub>12</sub>O<sub>40</sub>]*n*H<sub>2</sub>O (0.44 g, 0.15 mmol) and Co(OAc)<sub>2</sub>·4H<sub>2</sub>O (0.102 g, 0.4 mmol) was added and stirred for 0.5 h. The pH value of the hybrid solution was regulated to 1.8 by concentrated HNO<sub>3</sub> (10 μL). Then, the final suspension was transferred to a 23 mL Teflon-lined autoclave and heated at 130 °C for 4 days. After the solution was chilled, pink block crystals were obtained and filtered (82% yield based on W). The final pH value of the solution was 3.6. Anal. Calcd for C<sub>48</sub>H<sub>68</sub>N<sub>25</sub>O<sub>53</sub>BW<sub>12</sub>Co<sub>3</sub>: C 13.59, H 1.60, N 8.26, B 0.25, W 52.08, Co 4.17. Found: C 13.67, H 1.71, N 8.35, W 52.10, Co 4.15. Selected IR (solid KBr pellet, cm<sup>-1</sup>): 3445(w), 3126(m), 1610(m), 1523(s), 1423(m), 1381(w), 1349(w), 1280(s), 1207(m), 1128(s), 1016(m), 960(s), 912(s), 821(s). TG analysis reveals that the first weight loss ranging from 50 to 400 °C corresponds to the loss of four lattice and six coordinated water molecules (Figure S20).

**Procedure for Selective Oxidation of Styrene to Benzaldehyde.** In a typical case, styrene (0.25 mmol) and the catalyst (0.028 mmol) were dispersed in CH<sub>3</sub>CN (2 mL) and stirred for 5 min. Then, 30% H<sub>2</sub>O<sub>2</sub> (1 mmol) was injected into the above admixture and heated at 70 °C for 4–12 h. A small amount of the mixture was regularly removed and centrifuged. The filtrate was ascertained by GC and <sup>1</sup>H NMR analyses. After reaction, the catalyst was retrieved by centrifugation, washed with CH<sub>3</sub>CN, H<sub>2</sub>O, and C<sub>2</sub>H<sub>5</sub>OH alternately, and then dried in an oven at 70 °C for 24 h. For the recyclability experiments, the reactions were conducted under the same reaction conditions.

**X-ray Crystallography.** Crystallographic data for this paper have been deposited at the Cambridge Crystallographic Data Center: CCDC 1587315 for **1**, 1587314 for **2**. Crystal data and structural refinement for **1** and **2** are listed in Table 4. Selected bond lengths and angles of **1** and **2** are listed in Tables S2 and S4.

Table 4. Crystal Data and Structure Refinement for **1** and **2**

	<b>1</b>	<b>2</b>
formula	C <sub>24</sub> H <sub>47</sub> N <sub>12</sub> O <sub>50</sub> BW <sub>12</sub> Co	C <sub>48</sub> H <sub>68</sub> N <sub>25</sub> O <sub>53</sub> BW <sub>12</sub> Co <sub>3</sub>
<i>M<sub>r</sub></i>	3579.67	4237.07
<i>T</i> (K)	298(2)	298(2)
crystal system	monoclinic	triclinic
space group	C2/c	P $\bar{1}$
<i>a</i> (Å)	17.9972(7)	14.6466(5)
<i>b</i> (Å)	17.9935(6)	14.6578(7)
<i>c</i> (Å)	22.9940(13)	14.7089(7)
$\alpha$ (deg)	90	118.132(5)
$\beta$ (deg)	101.509(5)	100.992(3)
$\gamma$ (deg)	90	109.294(4)
<i>V</i> (Å <sup>3</sup> )	7296.5(6)	2389.92(18)
<i>Z</i>	4	1
$\mu$ (mm <sup>-1</sup> )	19.153	14.982
<i>F</i> (000)	6380	1929
reflns	14432	21419
<i>R<sub>int</sub></i>	0.0438	0.0409
GOF	1.059	1.006
<i>R<sub>1</sub></i> <sup>a</sup> [ <i>I</i> > 2σ( <i>I</i> )]	0.0802	0.0664
<i>wR<sub>2</sub></i> <sup>b</sup> (all data)	0.1955	0.1659

$${}^a R_1 = \sum ||F_o| - |F_c|| / \sum |F_o|. \quad {}^b wR_2 = \sum [w(F_o^2 - F_c^2)^2] / \sum [w(F_o^2)^2]^{1/2}.$$

## ■ ASSOCIATED CONTENT

### ● Supporting Information

The Supporting Information is available free of charge on the ACS Publications website at DOI: 10.1021/acs.inorgchem.8b00282.

Characterization methods and X-ray crystallography analysis (crystallographic collection and refinement

details), PXRD, FTIR, TG, UV–vis absorption spectra, selected bond lengths and angles, additional structures, and additional catalytic experiments (PDF)

### ■ Accession Codes

CCDC 1587314–1587315 contain the supplementary crystallographic data for this paper. These data can be obtained free of charge via [www.ccdc.cam.ac.uk/data\\_request/cif](http://www.ccdc.cam.ac.uk/data_request/cif), or by emailing [data\\_request@ccdc.cam.ac.uk](mailto:data_request@ccdc.cam.ac.uk), or by contacting The Cambridge Crystallographic Data Centre, 12 Union Road, Cambridge CB2 1EZ, UK; fax: +44 1223 336033.

## ■ AUTHOR INFORMATION

### Corresponding Authors

\*E-mail: [wangyh319@nenu.edu.cn](mailto:wangyh319@nenu.edu.cn).

\*E-mail: [tanhq870@nenu.edu.cn](mailto:tanhq870@nenu.edu.cn).

\*E-mail: [liyq658@nenu.edu.cn](mailto:liyq658@nenu.edu.cn).

### ORCID

Yangguang Li: 0000-0002-9696-8192

### Notes

The authors declare no competing financial interest.

## ■ ACKNOWLEDGMENTS

The authors gratefully acknowledge financial support from the National Natural Science Foundation of China (21671036 and 21771033), Fundamental Research Funds for the Central Universities (2412016KJ018), and the Opening Project of Key Laboratory of Polyoxometalate Science of the Ministry of Education (130028721).

## ■ REFERENCES

- (1) (a) Sun, M.; Zhang, J. Z.; Putaj, P.; Caps, V.; Lefebvre, F.; Pelletier, J.; Basset, J. M. Catalytic oxidation of light alkanes (C<sub>1</sub>–C<sub>4</sub>) by heteropoly compounds. *Chem. Rev.* **2014**, *114*, 981–1019. (b) Song, Y. F.; Long, D. L.; Ritchie, C.; Cronin, L. Nanoscale polyoxometalate-based inorganic/organic hybrids. *Chem. Rec.* **2011**, *11*, 158–171. (c) Liu, R. J.; Zhang, G. J.; Cao, H. B.; Zhang, S. J.; Xie, Y. B.; Haider, A.; Kortz, U.; Chen, B. H.; Dalal, N. S.; Zhao, Y. S.; Zhi, L. J.; Wu, C. X.; Su, Z. M.; Keita, B.; Yan, L.-K. Enhanced proton and electron reservoir abilities of polyoxometalate grafted on graphene for high-performance hydrogen evolution. *Energy Environ. Sci.* **2016**, *9*, 1012–1023. (d) Luo, W. J.; Hu, J.; Diao, H. L.; Schwarz, B.; Streb, C.; Song, Y. F. Robust polyoxometalate/nickel foam composite electrodes for sustained electrochemical oxygen evolution at high pH. *Angew. Chem., Int. Ed.* **2017**, *56*, 4941–4944. (e) Haviv, E.; Shimon, L. J. W.; Neumann, R. Photochemical reduction of CO<sub>2</sub> with visible light using a polyoxometalate as photoreductant. *Chem. - Eur. J.* **2017**, *23*, 92–95. (f) She, S.; Huang, Z. H.; Yin, P. C.; Bayaguud, A.; Jia, H. L.; Huang, Y. C.; Wei, Y.; Wei, Y. G. Buildup of redox-responsive hybrid from polyoxometalate and redox-active conducting oligomer: its self-assemblies with controllable morphologies. *Chem. - Eur. J.* **2017**, *23*, 14860–14865. (g) Wu, C. D.; Zhao, M. Incorporation of molecular catalysts in metal-organic framework for highly efficient heterogeneous catalysis. *Adv. Mater.* **2017**, *29*, 1605446.
- (2) (a) Zhao, M.; Zhang, X. W.; Wu, C. D. Structural transformation of porous polyoxometalate frameworks and highly efficient biomimetic aerobic oxidation of aliphatic alcohols. *ACS Catal.* **2017**, *7*, 6573–6580. (b) Liu, Y. W.; Luo, F.; Liu, S. M.; Liu, S. X.; Lai, X. Y.; Li, X. H.; Lu, Y.; Li, Y. G.; Hu, C. W.; Shi, Z.; Zheng, Z. P. Aminated graphene oxide impregnated with photocatalytic polyoxometalate for efficient adsorption of dye pollutants and its facile and complete photoregeneration. *Small* **2017**, *13*, 1603174. (c) Parrot, A.; Bernard, A.; Jacquart, A.; Serapian, S. A.; Bo, C.; Derat, E.; Oms, O.; Dolbecq, A.; Proust, A.; Métivier, R.; Mialane, P.; Izzet, G. Photochromism and dual-color fluorescence in a polyoxometalate-benzospiropyran molecular switch. *Angew. Chem., Int. Ed.* **2017**, *56*, 4872–4876. (d) Blasco-

- Ahicart, M.; Soriano-López, J.; Carbó, J. J.; Poblet, J. M.; Galan-Mascaros, J. R. Polyoxometalate electrocatalysts based on earth-abundant metals for efficient water oxidation in acid media. *Nat. Chem.* **2017**, *10*, 24–30.
- (3) Schultz, D. M.; Lévesque, F.; Dirocco, D. A.; Reibarkh, M.; Ji, Y. N.; Joyce, L. A.; Dropinski, J. F.; Sheng, H. M.; Sherry, B. D.; Davies, I. W. Oxyfunctionalization of the remote C-H bonds of aliphatic amines by decatungstate photocatalysis. *Angew. Chem., Int. Ed.* **2017**, *56*, 15274–15278.
- (4) (a) Buru, C. T.; Li, P.; Mehdi, B. L.; Dohnalkova, A.; Platero-Prats, A. E.; Browning, N. D.; Chapman, K. W.; Hupp, J. T.; Farha, O. K. Adsorption of a catalytically accessible polyoxometalate in a mesoporous channel-type metal-organic framework. *Chem. Mater.* **2017**, *29*, 5174–5181. (b) Du, J.; Cao, M. D.; Feng, S. L.; Su, F.; Sang, X. J.; Zhang, L. C.; You, W. S.; Yang, M.; Zhu, Z. M. Two new preyssler-type polyoxometalate-based coordination polymers and their application in horseradish peroxidase immobilization. *Chem. - Eur. J.* **2017**, *23*, 14614–14622.
- (5) (a) Mizuno, N.; Kamata, K. Catalytic oxidation of hydrocarbons with hydrogen peroxide by vanadium-based polyoxometalates. *Coord. Chem. Rev.* **2011**, *255*, 2358–2370. (b) Han, X. B.; Qin, C.; Wang, X. L.; Tan, Y. Z.; Zhao, X. J.; Wang, E. B. Bio-inspired assembly of cubane-adjustable polyoxometalate-based high-nuclear nickel clusters for visible light-driven hydrogen evolution. *Appl. Catal., B* **2017**, *211*, 349–356. (c) Shi, H. F.; Yu, Y. C.; Zhang, Y.; Feng, X. J.; Zhao, X. Y.; Tan, H. Q.; Khan, S. U.; Li, Y. G.; Wang, E. B. Polyoxometalate/TiO<sub>2</sub>/Ag composite nanofibers with enhanced photocatalytic performance under visible light. *Appl. Catal., B* **2018**, *221*, 280–289. (d) He, W. L.; Yang, X. L.; Zhao, M.; Wu, C. D. Suspending ionic single-atom catalysts in porphyrinic frameworks for highly efficient aerobic oxidation at room temperature. *J. Catal.* **2018**, *358*, 43–49.
- (6) (a) Dolbecq, A.; Dumas, E.; Mayer, C. R.; Mialane, P. Hybrid organic-inorganic polyoxometalate compounds: From structural diversity to applications. *Chem. Rev.* **2010**, *110*, 6009–6048. (b) Du, D. Y.; Qin, J. S.; Li, S. L.; Su, Z. M.; Lan, Y. Q. Recent advances in porous polyoxometalate-based metal-organic framework materials. *Chem. Soc. Rev.* **2014**, *43*, 4615–4632.
- (7) (a) Miras, H. N.; Vilà-Nadal, L.; Cronin, L. Polyoxometalate based open-frameworks (POM-OFs). *Chem. Soc. Rev.* **2014**, *43*, 5679–5699. (b) Wang, S. S.; Yang, G. Y. Recent advances in polyoxometalate-catalyzed reactions. *Chem. Rev.* **2015**, *115*, 4893–4962.
- (8) (a) An, H. Y.; Wang, E. B.; Xiao, D. R.; Li, Y. G.; Su, Z. M.; Xu, L. Chiral 3D architectures with helical channels constructed from polyoxometalate clusters and copper-amino acid complexes. *Angew. Chem.* **2006**, *118*, 918–922. (b) Zheng, S. T.; Zhang, J.; Yang, G. Y. Designed synthesis of POM-organic frameworks from {Ni<sub>6</sub>PW<sub>6</sub>} building blocks under hydrothermal conditions. *Angew. Chem., Int. Ed.* **2008**, *47*, 3909–3913. (c) Zheng, S. T.; Zhang, J.; Li, X. X.; Fang, W.; Yang, G. Y. Cubic polyoxometalate-organic molecular cage. *J. Am. Chem. Soc.* **2010**, *132*, 15102–15103. (d) Kuang, X. F.; Wu, X. Y.; Yu, R. M.; Donahue, J. P.; Huang, J. S.; Lu, C. Z. Assembly of a metal-organic framework by sextuple intercatenation of discrete adamantane-like cages. *Nat. Chem.* **2010**, *2*, 461–465.
- (9) (a) Jiao, Y. Q.; Zang, H. Y.; Wang, X. L.; Zhou, E. L.; Song, B. Q.; Wang, C. G.; Shao, K. Z.; Su, Z. M. Self-assembled arrays of polyoxometalate-based metal-organic nanotubes for proton conduction and magnetism. *Chem. Commun.* **2015**, *51*, 11313–11316. (b) Li, X. X.; Wang, Y. X.; Wang, R. H.; Cui, C. Y.; Tian, C. B.; Yang, G. Y. Designed assembly of heterometallic cluster organic frameworks based on anderson-type polyoxometalate clusters. *Angew. Chem., Int. Ed.* **2016**, *55*, 6462–6466. (c) Li, X. X.; Shen, F. C.; Liu, J.; Li, S. L.; Dong, L. Z.; Fu, Q.; Su, Z. M.; Lan, Y. Q. A highly stable polyoxometalate-based metal-organic framework with an ABW zeolite-like structure. *Chem. Commun.* **2017**, *53*, 10054–10057.
- (10) (a) Wei, T.; Zhang, M.; Wu, P.; Tang, Y. J.; Li, S. L.; Shen, F. C.; Wang, X. L.; Zhou, X. P.; Lan, Y. Q. POM-based metal-organic framework/reduced graphene oxide nanocomposites with hybrid behavior of battery-supercapacitor for superior lithium storage. *Nano Energy* **2017**, *34*, 205–214. (b) Sun, C. Y.; Liu, S. X.; Liang, D. D.; Shao, K. Z.; Ren, Y. H.; Su, Z. M. Highly stable crystalline catalysts based on a microporous metal-organic framework and polyoxometalates. *J. Am. Chem. Soc.* **2009**, *131*, 1883–1888. (c) Ma, F. J.; Liu, S. X.; Sun, C. Y.; Liang, D. D.; Ren, G. J.; Wei, F.; Chen, Y. G.; Su, Z. M. A sodalite-type porous metal-organic framework with polyoxometalate templates: Adsorption and decomposition of dimethyl methylphosphonate. *J. Am. Chem. Soc.* **2011**, *133*, 4178–4181. (d) Hao, X. L.; Ma, Y. Y.; Zang, H. Y.; Wang, Y. H.; Li, Y. G.; Wang, E. B. A polyoxometalate-encapsulating cationic metal-organic framework as a heterogeneous catalyst for desulfurization. *Chem. - Eur. J.* **2015**, *21*, 3778–3784. (e) Song, J.; Luo, Z.; Britt, D. K.; Furukawa, H.; Yaghi, O. M.; Hardcastle, K. I.; Hill, C. L. A multiunit catalyst with synergistic stability and reactivity: a polyoxometalate-metal organic framework for aerobic decontamination. *J. Am. Chem. Soc.* **2011**, *133*, 16839–16846.
- (11) (a) Fu, H.; Qin, C.; Lu, Y.; Zhang, Z. M.; Li, Y. G.; Su, Z. M.; Li, W. L.; Wang, E. B. An ionothermal synthetic approach to porous polyoxometalate-based metal-organic frameworks. *Angew. Chem., Int. Ed.* **2012**, *51*, 7985–7989. (b) Liu, D.; Lu, Y.; Tan, H. Q.; Chen, W. L.; Zhang, Z. M.; Li, Y. G.; Wang, E. B. Polyoxometalate-based purely inorganic porous frameworks with selective adsorption and oxidative catalysis functionalities. *Chem. Commun.* **2013**, *49*, 3673–3675. (c) Yan, J.; Zhou, W. Z.; Tan, H. Q.; Feng, X. J.; Wang, Y. H.; Li, Y. G. Ultrafine Ag/polyoxometalate-doped AgCl nanoparticles in metal-organic framework as efficient photocatalysts under visible light. *CrystEngComm* **2016**, *18*, 8762–8768. (d) Shi, D. Y.; He, C.; Qi, B.; Chen, C.; Niu, J. Y.; Duan, C. Y. Merging of the photocatalysis and copper catalysis in metal-organic frameworks for oxidative C-C bond formation. *Chem. Sci.* **2015**, *6*, 1035–1042.
- (12) (a) Han, Q. X.; Qi, B.; Ren, W. M.; He, C.; Niu, J. Y.; Duan, C. Y. Polyoxometalate-based homochiral metal-organic frameworks for tandem asymmetric transformation of cyclic carbonates from olefins. *Nat. Commun.* **2015**, *6*, 10007. (b) Nohra, B.; El Moll, H.; Rodriguez Albelo, L. M.; Mialane, P.; Marrot, J.; Mellot-Draznieks, C.; O’Keeffe, M.; Ngo Biboum, R.; Lemaire, J.; Keita, B.; Nadjo, L.; Dolbecq, A. Polyoxometalate-based metal organic frameworks (POMOFs): Structural trends, energetics, and high electrocatalytic efficiency for hydrogen evolution reaction. *J. Am. Chem. Soc.* **2011**, *133*, 13363–13374. (c) Yang, X. J.; Sun, M.; Zang, H. Y.; Ma, Y. Y.; Feng, X. J.; Tan, H. Q.; Wang, Y. H.; Li, Y. G. Hybrid coordination networks constructed from *ε*-Keggin-type polyoxometalates and rigid imidazole-based bridging ligands as new carriers for noble-metal catalysts. *Chem. - Asian J.* **2016**, *11*, 858–867. (d) Zhang, F. M.; Jin, Y.; Shi, J.; Zhong, Y. J.; Zhu, W. D.; El-Shall, M. S. Polyoxometalates confined in the mesoporous cages of metal-organic framework MIL-100 (Fe): Efficient heterogeneous catalysts for esterification and acetalization reactions. *Chem. Eng. J.* **2015**, *269*, 236–244.
- (13) (a) Qin, J. S.; Du, D. Y.; Guan, W.; Bo, X. J.; Li, Y. F.; Guo, L. P.; Su, Z. M.; Wang, Y. Y.; Lan, Y. Q.; Zhou, H. C. Ultrastable polymolybdate-based metal-organic frameworks as highly active electrocatalysts for hydrogen generation from water. *J. Am. Chem. Soc.* **2015**, *137*, 7169–7177. (b) Zhang, Z. M.; Zhang, T.; Wang, C.; Lin, Z. K.; Long, L. S.; Lin, W. Photosensitizing metal-organic framework enabling visible-light-driven proton reduction by a Wells-Dawson-type polyoxometalate. *J. Am. Chem. Soc.* **2015**, *137*, 3197–3200. (c) Kong, X. J.; Lin, Z. K.; Zhang, Z. M.; Zhang, T.; Lin, W. B. Hierarchical integration of photosensitizing metal-organic frameworks and nickel-containing polyoxometalates for efficient visible-light-driven hydrogen evolution. *Angew. Chem., Int. Ed.* **2016**, *55*, 6411–6416. (d) Boyd, T.; Mitchell, S. G.; Gabb, D.; Long, D. L.; Song, Y. F.; Cronin, L. POMzites: A family of zeolitic polyoxometalate frameworks from a minimal building block library. *J. Am. Chem. Soc.* **2017**, *139*, 5930–5938.
- (14) (a) Punniyamurthy, T.; Velusamy, S.; Iqbal, J. Recent advances in transition metal catalyzed oxidation of organic substrates with molecular oxygen. *Chem. Rev.* **2005**, *105*, 2329–2364. (b) Lee, D. G.; Chen, T. In *Comprehensive Organic Synthesis*; Pergamon Press: Oxford, U.K., 1991. (c) Larock, R. C. In *Comprehensive Organic Transformations*; Wiley-VCH: New York, 1999.

- (15) Yang, D.; Zhang, C. Ruthenium-catalyzed oxidative cleavage of olefins to aldehydes. *J. Org. Chem.* **2001**, *66*, 4814–4818.
- (16) (a) Gao, Q. S.; Giordano, C.; Antonietti, M. Biomimetic oxygen activation by MoS<sub>2</sub>/Ta<sub>3</sub>N<sub>5</sub> nanocomposites for selective aerobic oxidation. *Angew. Chem., Int. Ed.* **2012**, *51*, 11740–11744. (b) Liu, B.; Wang, P.; Lopes, A.; Jin, L.; Zhong, W.; Pei, Y.; Suib, S. L.; He, J. Au-carbon electronic interaction mediated selective oxidation of styrene. *ACS Catal.* **2017**, *7*, 3483–3488.
- (17) (a) Dhakshinamoorthy, A.; Alvaro, M.; Garcia, H. Aerobic oxidation of styrenes catalyzed by an iron metal organic framework. *ACS Catal.* **2011**, *1*, 836–840. (b) Rubinstein, A.; Jiménez-Lozano, P.; Carbó, J. J.; Poblet, J. M.; Neumann, R. Aerobic carbon-carbon bond cleavage of alkenes to aldehydes catalyzed by first-row transition-metal-substituted polyoxometalates in the presence of nitrogen dioxide. *J. Am. Chem. Soc.* **2014**, *136*, 10941–10948.
- (18) (a) Hu, J. L.; Li, K. X.; Li, W.; Ma, F. Y.; Guo, Y. H. Selective oxidation of styrene to benzaldehyde catalyzed by schiff base-modified ordered mesoporous silica materials impregnated with the transition metal-monosubstituted keggins-type polyoxometalates. *Appl. Catal., A* **2009**, *364*, 211–220. (b) Balula, S. S.; Cunha-Silva, L.; Santos, I. C. M. S.; Estrada, A. C.; Fernandes, A. C.; Cavaleiro, J. A. S.; Pires, J.; Freire, C.; Cavaleiro, A. M. V. Mono-substituted silicotungstates as active catalysts for sustainable oxidations: homo- and heterogeneous performance. *New J. Chem.* **2013**, *37*, 2341–2350.
- (19) (a) Tang, J.; Yang, X. L.; Zhang, X. W.; Wang, M.; Wu, C. D. A functionalized polyoxometalate solid for selective oxidation of styrene to benzaldehyde. *Dalton Trans.* **2010**, *39*, 3396–3399. (b) Kozhevnikov, I. V. Catalysis by heteropoly acids and multicomponent polyoxometalates in liquid-phase reactions. *Chem. Rev.* **1998**, *98*, 171–198.
- (20) Wang, D.; Astruc, D. The recent development of efficient earth-abundant transition-metal nanocatalysts. *Chem. Soc. Rev.* **2017**, *46*, 816–854.
- (21) (a) Masoomi, M. Y.; Bagheri, M.; Morsali, A. Application of two cobalt-based metal-organic frameworks as oxidative desulfurization catalysts. *Inorg. Chem.* **2015**, *54*, 11269–11275. (b) Zhu, J. J.; Kailasam, K.; Fischer, A.; Thomas, A. Supported cobalt oxide nanoparticles as catalyst for aerobic oxidation of alcohols in liquid phase. *ACS Catal.* **2011**, *1*, 342–347.
- (22) Spek, A. L. *PLATON, A Multipurpose Crystallographic Tool*; Utrecht University: Utrecht, The Netherlands, 1998.
- (23) (a) Jiang, G. X.; Chen, J.; Thu, H. Y.; Huang, J. S.; Zhu, N. Y.; Che, C. M. Ruthenium porphyrin-catalyzed aerobic oxidation of terminal aryl alkenes to aldehydes by a tandem epoxidation-isomerization pathway. *Angew. Chem., Int. Ed.* **2008**, *47*, 6638–6642. (b) Das, S.; Goswami, A.; Hesari, M.; Al-Sharab, J. F.; Mikmeková, E.; Maran, F.; Asefa, T. Reductive deprotection of monolayer protected nanoclusters: an efficient route to supported ultrasmall Au nanocatalysts for selective oxidation. *Small* **2014**, *10* (8), 1473–1478. (c) Duarte, T. A. G.; Estrada, A. C.; Simões, M. M. Q.; Santos, I. C. M. S.; Cavaleiro, A. M. V.; Neves, M. G. P. M. S.; Cavaleiro, J. A. S. Homogeneous catalytic oxidation of styrene and styrene derivatives with hydrogen peroxide in the presence of transition metal-substituted polyoxotungstates. *Catal. Sci. Technol.* **2015**, *5*, 351–363.
- (24) Patel, M. A.; Luo, F. X.; Khoshi, M. R.; Rabie, E.; Zhang, Q.; Flach, C. R.; Mendelsohn, R.; Garfunkel, E.; Szostak, M.; He, H. X. P-doped porous carbon as metal free catalysts for selective aerobic oxidation with an unexpected mechanism. *ACS Nano* **2016**, *10*, 2305–2315.
- (25) Chen, L. Y.; Chen, H. R.; Luque, R.; Li, Y. W. Metal-organic framework encapsulated Pd nanoparticles: towards advanced heterogeneous catalysts. *Chem. Sci.* **2014**, *5*, 3708–3714.
- (26) Gonzalez-de-Castro, A.; Xiao, J. L. Green and efficient: iron-catalyzed selective oxidation of olefins to carbonyls with O<sub>2</sub>. *J. Am. Chem. Soc.* **2015**, *137*, 8206–8218.
- (27) Mu, M. M.; Wang, Y. W.; Qin, Y. T.; Yan, X. L.; Li, Y.; Chen, L. G. Two-dimensional imine-linked covalent organic frameworks as a platform for selective oxidation of olefins. *ACS Appl. Mater. Interfaces* **2017**, *9*, 22856–22863.
- (28) Zhang, S. Y.; Zhang, Z. J.; Shi, W.; Zhao, B.; Cheng, P.; Liao, D. Z.; Yan, S. P. Structural evolution and magnetic properties of Co<sup>II</sup> coordination polymers varied from 1D to 3D. *Dalton Trans.* **2011**, *40*, 7993–8002.
- (29) Ma, Y. Y.; Tan, H. Q.; Wang, Y. H.; Hao, X. L.; Feng, X. J.; Zang, H. Y.; Li, Y. G. Polyoxometalate-based metal-organic coordination networks for heterogeneous catalytic desulfurization. *CrystEngComm* **2015**, *17*, 7938–7947.
- (30) Meng, X. R.; Song, Y. L.; Hou, H. W.; Han, H. Y.; Xiao, B.; Fan, Y. T.; Zhu, Y. Hydrothermal syntheses, crystal structures, and characteristics of a series of Cd-btx coordination polymers (btx = 1,4-Bis(triazol-1-ylmethyl)benzene. *Inorg. Chem.* **2004**, *43*, 3528–3536.
- (31) Rocchiccioli-Deltcheff, C.; Fournier, M.; Franck, R.; Thouvenot, R. Vibrational investigations of polyoxometalates. 2. Evidence for anion-anion interactions in molybdenum (VI) and tungsten (VI) compounds related to the Keggin structure. *Inorg. Chem.* **1983**, *22*, 207–216.